Environmental Science & Technology

pubs.acs.org/est

Article

Stabilization of Ferrihydrite and Lepidocrocite by Silicate during Fe(II)-Catalyzed Mineral Transformation: Impact on Particle Morphology and Silicate Distribution

Katrin Schulz, Laurel K. ThomasArrigo,* Ralf Kaegi, and Ruben Kretzschmar

Cite This: *Environ. Sci. Technol.* 2022, 56, 5929−5938

Read Online

ACCESS | Metrics & More | Article Recommendations | Supporting Information

ABSTRACT: Interactions between aqueous ferrous iron (Fe(II)) and secondary Fe oxyhydroxides catalyze mineral recrystallization and/or transformation processes in anoxic soils and sediments, where oxyanions, such as silicate, are abundant. However, the effect and the fate of silicate during Fe mineral recrystallization and transformation are not entirely understood and especially remain unclear for lepidocrocite. In this study, we reacted (Si-)ferrihydrite (Si/Fe = 0, 0.05, and 0.18) and (Si-)lepidocrocite (Si/Fe = 0 and 0.08) with isotopically labeled ^{57}Fe(II) (Fe(II)/Fe(III) = 0.02 and 0.2) at pH 7 for up to 4 weeks. We followed Fe mineral transformations with X-ray diffraction and tracked Fe atom exchange by measuring aqueous and solid phase Fe isotope fractions. Our results show that the extent of ferrihydrite transformation in the presence of Fe(II) was strongly influenced by the solid phase Si/Fe ratio, while increasing the Fe(II)/Fe(III) ratio (from 0.02 to 0.2) had only a minor effect. The presence of silicate increased the thickness of newly formed lepidocrocite crystallites, and elemental distribution maps of Fe(II)-reacted Si-ferrihydrites revealed that much more Si was associated with the remaining ferrihydrite than with the newly formed lepidocrocite. Pure lepidocrocite underwent recrystallization in the low Fe(II) treatment and transformed to magnetite at the high Fe(II)/Fe(III) ratio. Adsorbed silicate inactivated the lepidocrocite surfaces, which strongly reduced Fe atom exchange and inhibited mineral transformation. Collectively, the results of this study demonstrate that Fe(II)-catalyzed Si-ferrihydrite transformation leads to the redistribution of silicate in the solid phase and the formation of thicker lepidocrocite platelets, while lepidocrocite transformation can be completely inhibited by adsorbed silicate. Therefore, silicate is an important factor to include when considering Fe mineral dynamics in soils under reducing conditions.

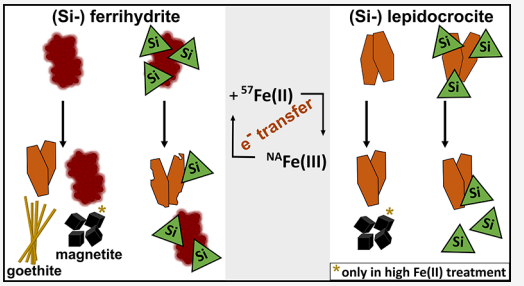

KEYWORDS: *iron, goethite, magnetite, atom exchange, redox, crystal morphology, elemental mapping*

INTRODUCTION

Secondary oxides and oxyhydroxides of iron (Fe) are important sorbents for nutrients and contaminants in soils, influencing the chemical speciation and behavior of these elements.[1−3] In sub- or anoxic soils, dissimilatory Fe(III) reduction generates aqueous Fe(II). Interactions between Fe(II) and secondary Fe oxyhydroxides, such as ferrihydrite ($Fe_5HO_8{\cdot}4H_2O$) and lepidocrocite (γ-FeO(OH)), catalyze mineral recrystallization and transformation to more crystalline Fe minerals.[4−6] During the interaction of Fe(II) with Fe oxyhydroxides, adsorbed Fe(II) can be oxidized to Fe(III), leading to the reduction of structural Fe(III) through electron transfer and its release as Fe(II) into solution.[7,8] Thereby, Fe atoms are exchanged between the solid and the aqueous phase.[7,8] Recently, Sheng et al.[9] suggested that the accumulation of a labile Fe(III) species on the ferrihydrite surface may lead to the nucleation of ferrihydrite transformation products. Ferrihydrite interaction with Fe(II) leads to its transformation to lepidocrocite, goethite (α-FeOOH), and/or magnetite (Fe_3O_4), depending on the reaction conditions.[4,5] Model experiments have shown that the mineral products from ferrihydrite transformation are influenced by the Fe(II) concentration,[4,5] the Fe(II)/Fe(III) ratio,[4,5] pH,[10,11] temperature,[11] the solid to solution ratio,[12] and the ligand and buffer choice.[4] For example, while Fe(II)-catalyzed ferrihydrite transformation at pH <7 favors the formation of lepidocrocite and goethite,[4,5] high Fe(II) concentrations and pH >7 lead to the formation of magnetite.[4,10] During the Fe(II)-catalyzed transformation of ferrihydrite to goethite and magnetite, lepidocrocite often occurs as an intermediate phase[4,5,13] but has rarely been studied on its own (e.g., refs 4, 6, 14, and 15). Some studies have shown lepidocrocite transformation to

Received: December 23, 2021
Revised: March 25, 2022
Accepted: March 30, 2022
Published: April 18, 2022

goethite[4,14] or magnetite;[6,15] however, results published to date are inconclusive, most likely due to the differences between experimental conditions (e.g., pH, Fe(II)/Fe(III) ratios, ligand, and buffer choice)[4] as well as variations in lepidocrocite particle size.[6] These results show that the stability of lepidocrocite during the interaction with Fe(II) and its role as an intermediate phase during the Fe(II)-catalyzed transformation of ferrihydrite is still poorly understood and warrants further investigation.

In natural environments, oxyanions, such as arsenic, phosphate, and silicate, and organic matter are abundant and can influence the formation and transformation of Fe oxyhydroxides in soils.[13,16−21] For example, Fe(II)-catalyzed transformation of ferrihydrite is hindered in the presence of arsenic[16] and coprecipitated organic matter.[13] Additionally, during the biomineralization of ferrihydrite, adsorbed phosphate reduced the mineral transformation rate and altered mineral transformation pathways compared to phosphate-free ferrihydrite.[17] However, the role of silicate during mineral transformations is less studied. Aqueous orthosilicate (H_4SiO_4) is ubiquitous in soil and sediment pore waters since silicate anions are released by chemical weathering of silicate minerals. Silicate anions interact with the positively charged surfaces of Fe oxyhydroxides at circumneutral pH and can coprecipitate with ferrihydrite, resulting in smaller crystallite sizes compared to pure ferrihydrite.[19,22,23] During Fe(III) hydrolysis, silicate has been reported to bind to free corner sites of FeO_6 octahedra, hindering the formation of Fe oxyhydroxide polymeric complexes,[24] which may explain the smaller ferrihydrite crystallite sizes when formed in the presence of silicate. Nonetheless, ferrihydrite can precipitate at Si/Fe ratios of up to 0.68,[19] where silicate is integrated into micropores of ferrihydrite aggregates but not incorporated into the mineral structure.[25] In contrast, lepidocrocite formation is hindered at Si/Fe ratios >0.015,[21] and silicate-bearing ferrihydrite (Si-ferrihydrite) will precipitate instead.[21,26,27] Therefore, aqueous silicate in natural systems is likely adsorbed to lepidocrocite surfaces, whereas it is integrated into ferrihydrite aggregates. The reactivity and transformation of Si-ferrihydrites were studied by Jones et al.[18] who reacted Si-ferrihydrite coprecipitates with Fe(II) (Fe(II)/Fe(III) = 0.4 and Si/Fe(III) = 0.68) and observed complete Fe atom exchange (IAE) within 1 week but no transformation of Si-ferrihydrite coprecipitates. Similarly, they found that the presence of aqueous silicate can strongly reduce the IAE and mineral transformation of ferrihydrite and lepidocrocite during the reaction with Fe(II).[18] However, the effects of solid-associated silicate at low (<0.2) Si/Fe ratios and low (≤0.2) Fe(II)/Fe(III) ratios are not well studied. Especially for lepidocrocite formation, recrystallization, and/or transformation, the implications of solid-associated silicate remain unclear. Furthermore, the spatial redistribution of silicate in the solid phase during these processes, which may impact trace element sorption (e.g., As[22]), has not been investigated to date. Because ferrihydrite and lepidocrocite are closely linked to the biogeochemical cycling of nutrients and contaminants, we need to understand their reactivity in natural systems.

Therefore, we (i) examined the effects of solid-associated silicate on the stability and reactivity of ferrihydrite and lepidocrocite upon the reaction with Fe(II) and (ii) tracked the release of silicate to the aqueous phase and its spatial distribution in the solid phase. To this end, we reacted pure and silicate-associated ferrihydrite and lepidocrocite with isotopically labeled ^{57}Fe(II) at pH 7 for 4 weeks, tracking trends in aqueous Fe and Si and the IAE between aqueous Fe(II) and structural Fe(III). In comparison to previous studies,[4,6,18] we chose low Fe(II)/Fe(III) ratios (≤0.2) and low Si/Fe ratios (0.05−0.18), which we consider relevant to natural environments. To better understand the impact of silicate on mineral transformation products, we also followed the kinetics of mineral transformations and characterized the products in terms of mineral morphology and changes in spatial silicate distribution.

MATERIALS AND METHODS

Mineral Synthesis and Characterization. All reagents were prepared with doubly deionized (DDI) water (>18.2 MΩ·cm, Milli-Q, Millipore, Merck), and minerals were synthesized from isotopically natural-abundant (NA) Fe salts (5.8% ^{54}Fe, 91.7% ^{56}Fe, 2.2% ^{57}Fe, and 0.3% ^{58}Fe).[28] Ferrihydrite (Fh) was synthesized using the method of Schwertmann and Cornell.[29] In brief, a 0.2 M ferric nitrate ($Fe(NO_3)_3{\cdot}9H_2O$) solution (pH ∼1) was titrated (836 Titrando, Metrohm) with 1 M NaOH (Titrisol, Merck) to pH 7.5 ± 0.1 under vigorous stirring at room temperature. The Si-ferrihydrite coprecipitates were synthesized after Cismasu et al.[19] with slight modifications. The synthesis procedure followed that of ferrihydrite but used a NaOH solution containing 16.7 or 66.7 mM Si, added as sodium metasilicate granules (Na_2SiO_3, Sigma-Aldrich). Appropriate volumes of silicate-doped NaOH were added to the ferric nitrate solution to reach nominal Si/Fe ratios of 0.05 and 0.25, respectively. The pH of the resulting suspension was monitored and adjusted with silicate-free NaOH for 1 h after completion of the titration, and the Si-ferrihydrite suspensions were equilibrated in the dark for 24 h. The (Si-)ferrihydrite precipitates were centrifuge-washed with DDI water three times, shock-frozen dropwise in liquid N_2, freeze-dried, and gently homogenized with a mortar and pestle. The shock-freezing was applied to ensure a fast and homogeneous freezing process of the precipitates, which reduces the formation of large and dense ferrihydrite aggregates.[30] Lepidocrocite (Lp) was synthesized using the method of Schwertmann and Cornell[29] with slight modifications. A 0.2 M Fe(II) solution (300 mL) prepared from $FeCl_2$ was titrated to pH 6.7−6.9 with 1 M NaOH at room temperature and oxidized under vigorous stirring and gentle purging with air (approximately 400 mL min^{-1}) for ∼90 min. The precipitates were washed, shock-frozen, freeze-dried, and homogenized, as described above.

To obtain silicate-adsorbed lepidocrocite, 1 g of the dried lepidocrocite was resuspended in 200 mL of a 13 mM Si solution to reach a final Si/Fe ratio of 0.23. The silicate was spiked in the form of an alkaline stock solution (200 mM Si), derived from Na_2SiO_3 dissolved in DDI water, and the pH of the suspension was adjusted to 7.5 with 1 M HCl (Suprapur). Due to the high silicate concentration, visible white flocs (up to 3 mm) formed after 48 h of equilibration under gentle stirring. The flocs were removed by passing the suspension through a 200 μm sieve. The silicate-adsorbed lepidocrocite was washed and freeze-dried as described above. Total Fe and Si contents in the mineral phases were analyzed after dissolution in concentrated HCl at room temperature with inductively coupled plasma optical emission spectrometry (ICP-OES). All mineral phases were characterized by X-ray diffraction (XRD), Fourier-transform infrared spectroscopy

https://doi.org/10.1021/acs.est.1c08789
Environ. Sci. Technol. 2022, 56, 5929−5938

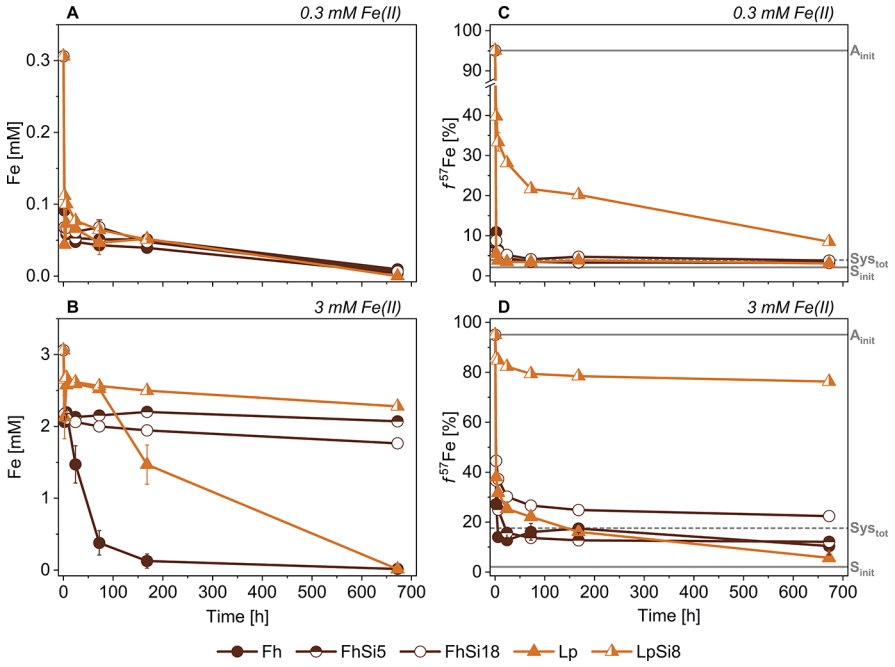

Figure 1. Aqueous iron (Fe) concentrations (A, B) and ^{57}Fe isotope fractions (f^{57}Fe; C, D) in suspensions spiked with 0.3 mM (A, C) and 3 mM Fe(II) (B, D). Gray solid lines in panels (C, D) represent the f^{57}Fe of the initial aqueous phase (A_{init}) and unreacted solids (S_{init}), and the dashed gray line shows the calculated f^{57}Fe of the total system (Sys_{tot}). Error bars show the standard error of experimental triplicates, and errors <5% (A, B) and <1% (C, D) are smaller than the symbols and are not shown. 672 h = 4 weeks. This data and a detailed view of the first 6 h can be found in Section S4.

(FTIR), scanning transmission electron microscopy (STEM), and multipoint N_2-BET (Brunauer–Emmett–Teller)[31] surface area analysis. Details of these methods are given in Section S1 of the Supporting Information.

The XRD analysis confirmed the expected mineralogical composition of the pure and silicate-associated ferrihydrites and lepidocrocites, without detecting mineral impurities (Section S1). The Si/Fe ratios in the Si-ferrihydrites were 0.05 and 0.18, named FhSi5 and FhSi18, respectively. For the Si-adsorbed lepidocrocite, the Si/Fe ratio was 0.08, from here on named LpSi8. Secondary electron images showed that Fh and FhSi5 consisted of nanometer-sized, spherical ferrihydrite particles in dense micrometer-sized aggregates (Section S9), and Lp and LpSi8 crystallites were lath- and finger-shaped (Section S9), which agrees with previous observations for ferrihydrite[4,32] and lepidocrocite.[4,14,32]

^{57}Fe(II) Spike Experiments. All solutions were degassed with nitrogen (N_2) for at least 1 h prior to transfer into an anoxic glovebox (N_2 atmosphere, <5 ppm O_2). All solutions, chemicals, equipment, and precipitates were equilibrated in the glovebox for at least 1 day before use. Suspensions of Fh, FhSi5, FhSi18, Lp, and LpSi8 containing 15 mM Fe(III) in 85 mL of anoxic 3-(*N*-morpholino)propanesulfonic acid (MOPS) buffer (50 mM, pH 7) were prepared in 100 mL septum glass bottles (in triplicates) and equilibrated inside the glovebox overnight. The corresponding solid to solution ratios were between 1.4 and 1.7 g L^{-1}, depending on the Fe content of the respective materials (Section S2). An Fe(II) stock solution was prepared by dissolving isotopically labeled zero valent Fe (95.08% ^{57}Fe, Isoflex USA) in 3.5 M HCl (Suprapur) overnight. The solution was passed through a 0.45 μm nylon filter and diluted to 0.2 M Fe. The ^{57}Fe(II) concentration in the stock solution was determined by the 1,10-phenanthroline method after Walter[33] using UV–visible spectroscopy (λ = 510 nm). Aliquots of the ^{57}Fe(II) solution were added to the mineral suspensions to achieve final Fe(II) concentrations of 0.3 mM (low Fe(II)) and 3 mM (high Fe(II)), corresponding to final Fe(II)/Fe(III) ratios of 0.02 and 0.2 (for low and high Fe(II) treatments, respectively). The pH was measured in all suspensions immediately after adding the ^{57}Fe(II). In the first 5 min, suspensions of the high Fe(II) treatment were amended with 1 M NaOH (<200 μL) to readjust pH. Thereafter, the suspension pH remained constant at 7.0 ± 0.1. All bottles were crimp-sealed with a butyl rubber stopper and shaken (~15 rpm) in the dark in an overhead shaker outside the glovebox. Control bottles containing the mineral phases in buffer solution without the Fe(II) spike were included to consider mineral transformation or dissolution in the absence of Fe(II).

At 2, 6, 24, 72, 168 (1 week), and 672 h (4 weeks) after the ^{57}Fe(II) spike, septum bottles were returned to the glovebox for aqueous and solid phase sampling. Reactors were vigorously shaken until the solid phase was completely resuspended before the crimp-sealed bottles were opened, and an aliquot of the suspension was passed through a 0.45 μm nylon filter. Samples for aqueous phase analyses were additionally passed through a 0.22 μm nylon filter. The residual solid phase (≥0.45 μm) on the filter was rinsed with 3 mL of DDI water and dried in the glovebox in the dark. Solid phase triplicates were combined for analyses by manual homogenization. After sampling, the bottles were again crimp-sealed, removed from the glovebox, and returned to the shaker.

Aqueous Phase Analyses. Aqueous Fe concentrations in the 0.22 μm filtrates were measured by ICP-OES, and the dominance of Fe(II) over Fe(III) in solution was confirmed in 4 week samples (median: 99% Fe(II)) by the 1,10-phenanthroline method.[33] Therefore, all reported values for Fe(II) refer to total aqueous Fe. Aqueous Si concentrations

https://doi.org/10.1021/acs.est.1c08789
Environ. Sci. Technol. 2022, 56, 5929–5938

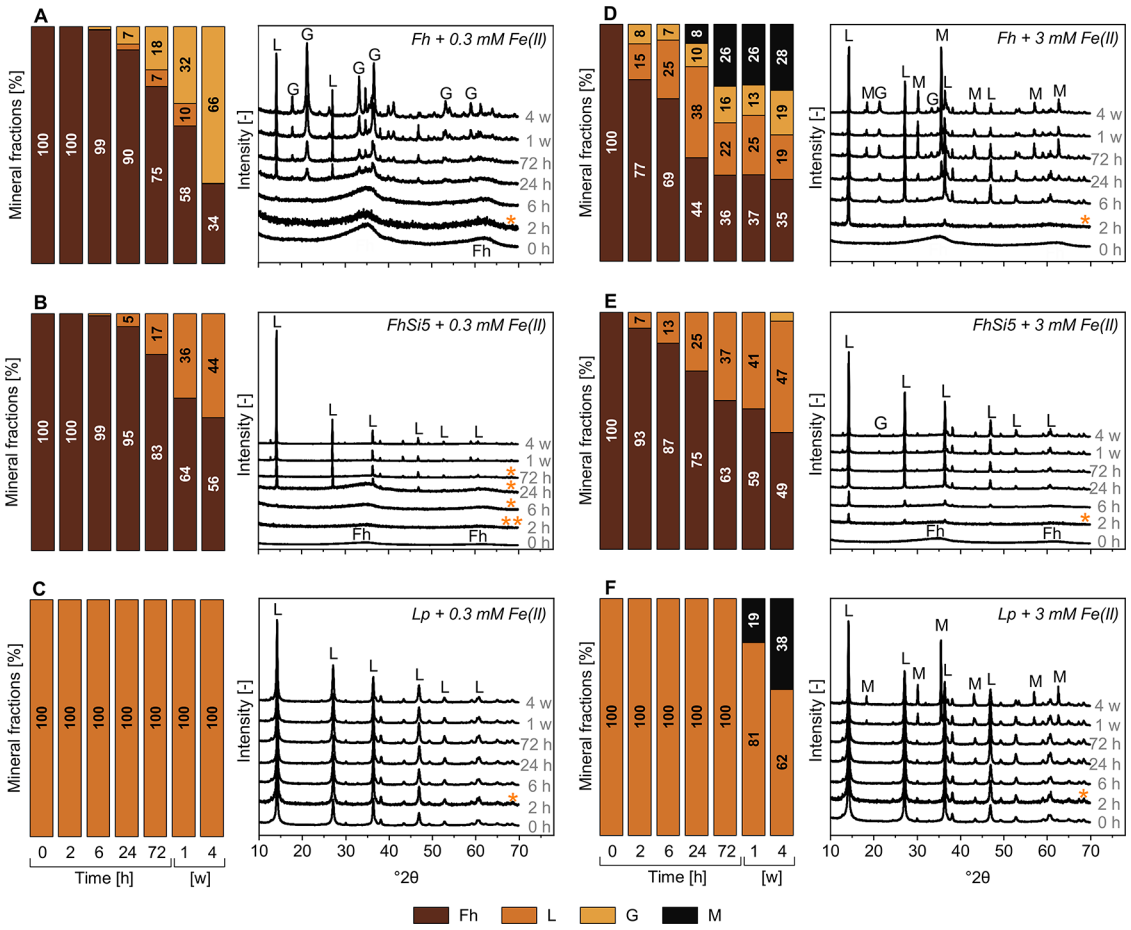

Figure 2. Mineral phase fractions of solid samples before and during the reaction with 0.3 mM Fe(II) (A−C) and 3 mM Fe(II) (D−F) at six time points (h = hours, w = weeks) over 4 weeks (= 672 h), derived from X-ray diffraction patterns. Fractions <5% are not labeled but are reported with Rietveld fit data in Section S7. Main diffraction peaks are labeled with mineral abbreviations: Fh = ferrihydrite, L = lepidocrocite, G = goethite, M = magnetite. The marked XRD patterns were scaled by 5 (*) or 10 (**) in this figure. Corresponding figures for FhSi18 and LpSi8 are found in Section S7. Iron(II)-free control reactors showed no signs of mineral transformation (Section S7).

and Fe isotope ratios in the 0.22 μm filtrates were measured with triple-quadrupole inductively coupled plasma mass spectrometry (ICP-MS), and ^{57}Fe isotope fractions (f^{57}Fe) were calculated relative to the sum of ^{54}Fe, ^{56}Fe, ^{57}Fe, and ^{58}Fe (details and quality controls in Section S3).

Solid Phase Analyses. The reacted solid phases were analyzed by XRD, and mineral phase fractions were determined by Rietveld quantitative phase analysis of the diffractograms, where ferrihydrite was included as a mass-calibrated PONKCS[34] phase (Section S6).[10,13] The Fe isotope composition of the reacted solid phases was determined after dissolution in HCl by ICP-MS. For the Fe isotope analysis, approximately 10 mg of the sample was dissolved in 1 mL of concentrated HCl in 2 mL Eppendorf plastic tubes and subsequently diluted to 30 mL with DDI water. The morphology of the transformation products and spatial distribution of Fe and Si in the solid phases were studied on selected 4 week reacted samples using STEM coupled with energy-dispersive X-ray analysis (EDX; details in Section S9).

RESULTS AND DISCUSSION

Aqueous Fe(II) and Fe Atom Exchange. Temporal trends in aqueous Fe(II) concentrations showed that Fe(II) was rapidly removed from solution in all suspensions (Figure 1A,B and Section S4). Within the first 2 h, >0.2 mM of the initially spiked 0.3 mM Fe(II) and ∼1 mM of the initially spiked 3 mM Fe(II) were removed from solution in the pure Fh and Lp suspensions. At the same time, the aqueous f^{57}Fe decreased similarly rapidly in Fh and Lp suspensions in the low and the high Fe(II) treatment (Figure 1C,D). This indicates that sorbed ^{57}Fe(II) was oxidized by the transfer of an electron to the sorbent solid phase, resulting in the reduction and release of ^{NA}Fe(III) as ^{NA}Fe(II) to the solution. Adsorption of the ^{57}Fe(II) alone would not lead to a detectable change in the Fe isotope composition of the aqueous phase. Within 2 h of reaction in the low Fe(II) treatment, the aqueous f^{57}Fe in Fh (10.8%) and Lp (5.5%) suspensions dropped sharply and approached the isotopic composition of the total system (f^{57}Fe = 3.9%), demonstrating that rapid atom exchange between aqueous ^{57}Fe(II) and structural ^{NA}Fe(III) in the solid phase occurred (Figure 1C). Similarly, in the high Fe(II) treatment, the aqueous f^{57}Fe in the Fh (27.2%) and Lp (38.0%) suspensions approached the isotopic composition of the total system (f^{57}Fe = 17.6%) within 2 h (Figure 1D).

After the first 2 h, Fe(II) concentrations in the low Fe(II) treatment continued to decrease slowly, and after 4 weeks, the Fe(II) concentrations were <40 μM in the Fh and Lp suspensions (Figure 1A). The aqueous f^{57}Fe in low Fe(II) Fh and Lp suspensions matched the isotopic composition of the total system at 4 weeks (Figure 1C). In the high Fe(II)

https://doi.org/10.1021/acs.est.1c08789
Environ. Sci. Technol. 2022, 56, 5929−5938

treatments, the Fe(II) concentration decreased sharply in Fh and Lp suspensions starting between 6 and 24 h and between 72 and 168 h, respectively (Figure 1B). After 4 weeks, Fe(II) concentrations were <20 μM in the Fh and Lp suspensions. The aqueous f^{57}Fe after 4 weeks in the high Fe(II) Fh and Lp suspensions was lower than the isotopic composition of the total system (Figure 1D), suggesting that the solid phase became enriched in ^{57}Fe, potentially in surface-associated crystalline products from Fh and Lp transformation.[13]

Coprecipitated silicate in FhSi5 and FhSi18 did not result in differences in Fe(II) removal from solution or IAE in the low Fe(II) treatment compared to pure Fh, whereas adsorbed silicate on LpSi8 resulted in slightly reduced Fe(II) adsorption and slower IAE (Figure 1A,C). In the high Fe(II) treatment, Fe(II) removal was similar for silicate-associated minerals (FhSi5, FhSi18, and LpSi8) compared to their corresponding pure mineral phases (Fh and Lp) in the first 6 h (Figure 1B). The impact of silicate became clearer after 24 h, where Fe(II) concentrations in the silicate-associated mineral suspensions (FhSi5, FhSi18, and LpSi8) remained relatively stable until 4 weeks, compared to a decrease in Fe(II) in pure Fh and Lp suspensions. After 4 weeks of reaction in the high Fe(II) treatment, the Fe(II) concentrations in the FhSi5 and FhSi18 suspensions were 2.1 and 1.8 mM, respectively. In comparison, the Fe(II) concentration in theLpSi8 suspension was 2.3 mM after 4 weeks (Figure 1B). The extent of IAE in the high Fe(II) treatment was similar for FhSi5 compared to pure Fh and only slightly reduced for FhSi18 (Figure 1D). Similarly rapid IAE has been reported for pure ferrihydrite[13] and Si-ferrihydrite coprecipitates up to a Si/Fe ratio of 0.68.[18] In contrast, IAE was strongly hindered by surface-adsorbed silicate in LpSi8, where the aqueous f^{57}Fe was 76.3% at 4 weeks in the high Fe(II) treatment, indicating that only a minor fraction of aqueous ^{57}Fe(II) exchanged with LpSi8 and that adsorbed silicate can reduce lepidocrocite reactivity (Figure 1D). Collectively, these results show that IAE is similarly rapid in pure Lp compared to pure Fh and that IAE is only slightly reduced by coprecipitated silicate in ferrihydrite (up to Si/Fe = 0.18) yet is strongly hindered by the presence of surface-adsorbed silicate in lepidocrocite.

Aqueous Silicate. Silicate was released from FhSi5, FhSi18, and LpSi8 to the aqueous phase within 2 h of reaction in both the low and the high Fe(II) treatment (relative Si release = 3% (FhSi5 and FhSi18) or 30% (LpSi8); Section S5). Within 4 weeks, the relative Si release from FhSi5 increased to 14 and 8% in the low and the high Fe(II) treatment, respectively. The aqueous Si fractions in FhSi18 suspensions, however, remained relatively stable after 2 h (3−5%). In comparison, the relative Si release from LpSi8 within 4 weeks of reaction in the low (58% of Si) and the high (46% of Si) Fe(II) treatment was much higher than from FhSi5 and FhSi18. This is likely related to the fact that silicate adsorbed to external mineral surfaces in LpSi8 but adsorbed to both external and internal surfaces (e.g., in micropores) of FhSi5 and FhSi18 aggregates during coprecipitation. Therefore, the silicate in FhSi5 and FhSi18 aggregates could only be released by mineral dissolution or micropore diffusion of silicate out of the aggregates, whereas silicate on the LpSi8 surface may desorb more rapidly. Furthermore, based on the specific surface area of each mineral (Section S1), the estimated relative coverage of the mineral surface by silicate was higher in the LpSi8 (~19 μmol Si m^{-2}) than in FhSi5 (~4 μmol Si m^{-2}) and FhSi18 (~13 μmol Si m^{-2}). As the BET specific surface area may be impacted by the aggregation of particles during flash-freezing and freeze drying,[30] the stated Si surface loadings might be slightly overestimated. However, the higher surface loading of LpSi8 likely facilitated silicate release despite some polymerization of silicate on the mineral surfaces, as shown by infrared spectroscopy (Section S1).

Mineral Transformation in the Absence of Silicate. The mineral fractions in reacted samples determined from Rietveld analysis of XRD data showed that, after the addition of Fe(II), Fh transformed into crystalline mineral phases within a few hours (Figure 2 and Section S7). Within 6 h of reaction in the low Fe(II) treatment, traces of lepidocrocite (~1%) were observed in the XRD patterns (e.g., small peaks at 14.14° 2θ (d = 6.269 Å) and 27.05° 2θ (d = 3.296 Å); Figure 2A). Thereafter, Fh transformation to lepidocrocite continued, reaching a maximum lepidocrocite contribution in the low Fe(II) Fh suspension of 10% at 1 week before decreasing to below the detection limit at 4 weeks. In contrast, goethite started to form within 24 h and dominated the transformation products until the end of the experiment, where 66% of Fh had transformed to goethite (Figure 2A). In the 3 mM Fe(II) treatment, the higher Fe(II) concentration facilitated faster transformation of Fh and enabled magnetite formation (Figure 2D). Lepidocrocite formation from Fh already started within less than 2 h in the high Fe(II) treatment and was the dominant transformation product until it reached its maximum at 24 h (38%). Thereafter, lepidocrocite contributions decreased at the expense of goethite and magnetite formation. During 4 weeks of reaction in the high Fe(II) treatment, Fh transformed to a mixture of lepidocrocite (19%), goethite (19%), and magnetite (28%), with 35% ferrihydrite remaining (Figure 2D). Based on the rapid IAE recorded in the Fh suspensions (Figure 1C,D), this remaining ferrihydrite may have recrystallized. The onset of magnetite accumulation between 6 and 24 h agrees well with the rapid removal of aqueous Fe(II) starting after 6 h (Figures 1B and 2D). Hansel et al.[4,35] suggested that magnetite accumulation can make the dissolution reprecipitation reaction from ferrihydrite to goethite less favorable due to the greater thermodynamic stability of magnetite. This agrees with our observation that the goethite fraction in the high Fe(II) Fh suspension only increased from 10 to 16% between 24 and 72 h, while the magnetite fraction increased from 8 to 26% (Figure 2D). After 72 h, the mineral composition in the high Fe(II) Fh suspension remained relatively constant until the end of the experiment, with 35−37% ferrihydrite, 19−25% lepidocrocite, 13−19% goethite, and 26−28% magnetite (Figure 2D). In general, the transformation of Fh into lepidocrocite, goethite, and magnetite during reactions with Fe(II) agrees well with the rapid IAE (Figure 1C,D).

The Lp did not transform to more crystalline mineral phases in the low Fe(II) treatment over 4 weeks (Figure 2C). Combined with extensive Fe(II) uptake and rapid IAE recorded for Lp in the low Fe(II) treatment (Figure 1A,C), this suggests that Lp underwent recrystallization rather than transformation. Mineral recrystallization has also been reported for Fe(II) interactions with other crystalline Fe minerals (e.g., goethite[36,37] and hematite[38]). In contrast, during the reaction in the high Fe(II) treatment, 38% of Lp transformed to magnetite within 4 weeks without indication of goethite formation (Figure 2F). Whether lepidocrocite undergoes recrystallization versus transformation may be controlled by the supersaturation of labile Fe(III) on the lepidocrocite

https://doi.org/10.1021/acs.est.1c08789
Environ. Sci. Technol. 2022, 56, 5929−5938

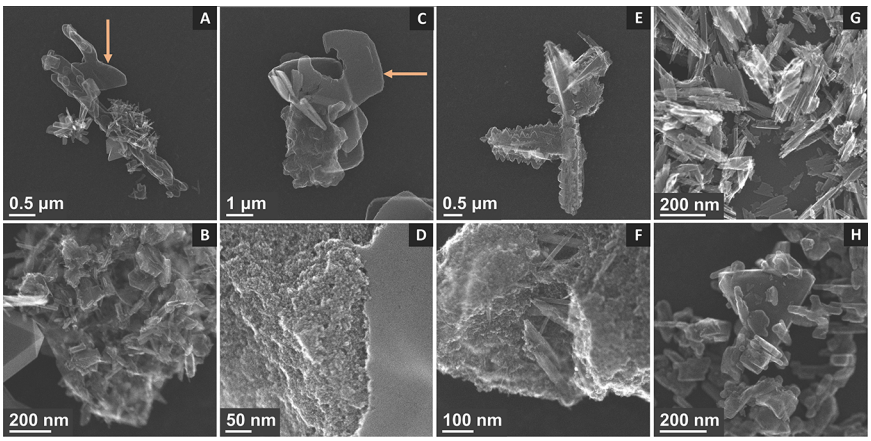

Figure 3. Secondary electron images of Fh reacted with 3 mM Fe(II) (A, B), FhSi5 reacted with 0.3 mM Fe(II) (C, D), FhSi5 reacted with 3 mM Fe(II) (E, F), unreacted Lp (G), and Lp reacted with 3 mM Fe(II) (H); all reacted samples are 4 week samples, and scales are given in the respective images. The arrows point toward a <1 μm lepidocrocite platelet with a poorly defined crystal habit (A) and a micrometer-sized lepidocrocite platelet with a well-defined crystal habit (C). Additional images of FhSi5 reacted with 0.3 mM Fe(II) and of unreacted Fh and FhSi5 are found in Section S9.

surface.[9,12] The transformation of lepidocrocite to magnetite occurs through a dissolution reprecipitation mechanism[15] and agrees with observations of magnetite accumulation during lepidocrocite interactions with Fe(II) at higher Fe(II)/Fe(III) ratios than used in this study (e.g., 2 at pH 6.5 in Pedersen et al.[6] versus 0.02 and 0.2 at pH 7 in this study; Section S2). However, the absence of goethite formation from lepidocrocite contrasts the strong dominance of goethite in transformation products originating from Fe(II)-reacted Fh in the low Fe(II) treatment. During Fh transformation, goethite may have nucleated from Fh and then, due to its greater thermodynamic stability, continued to grow at the expense of lepidocrocite. These results indicate that goethite nucleates more easily from Fh than from Lp under the given experimental conditions (Section S2), whereas magnetite can be formed from both Fh and Lp. This may be explained by the lower nucleation energy barrier for goethite formation from ferrihydrite than from lepidocrocite and the lower nucleation energy barrier for magnetite than goethite formation from lepidocrocite.[39] Few studies have reported goethite formation from lepidocrocite. For example, Yan et al.[14] found goethite and magnetite formation from lepidocrocite at low Fe(II)/Fe(III) ratios (0.02−0.06) but with strongly drifting pH values (7−3.7). Hansel et al.[4] found goethite but no magnetite formation from lepidocrocite-coated sand at high Fe(II)/Fe(III) ratios (0.8 and 8) at pH 7.2. However, this also demonstrated that the amount of goethite formed from lepidocrocite can vary widely (4−32%) depending on the Fe(II) concentration, ligand choice (chloride and sulfate), and buffer type (PIPES and bicarbonate).[4] Collectively, these results suggest that goethite formation from pure lepidocrocite is less favorable than from ferrihydrite and that ferrihydrite may provide the main goethite nucleation sites in mixed mineral systems.

Mineral Transformation in the Presence of Silicate. The mineral phase fractions during and after the reaction of Si-ferrihydrites (FhSi5 and FhSi18) with Fe(II) showed that coprecipitated silicate hindered the Fe(II)-catalyzed formation of crystalline minerals in both Fe(II) treatments and at both silicate loadings (Figure 2B,E and Section S7). The reaction of FhSi5 in the low Fe(II) treatment for 4 weeks resulted in the transformation to lepidocrocite (44%), with lepidocrocite first detected at 6 h (Figure 2B). In the high Fe(II) treatment, lepidocrocite (47%) was the major transformation product, with traces of goethite (4%) appearing at 4 weeks (Figure 2E). The reaction of FhSi18 in the low Fe(II) treatment resulted in no mineral transformation, while after the reaction in the high Fe(II) treatment for 4 weeks, traces of lepidocrocite (4%) and goethite (2%) were present (Section S7). In combination with the higher relative Si release from FhSi5 than from FhSi18 (Section S5), this suggests that the larger extent of mineral transformation (~45% in FhSi5, <7% in FhSi18) led to higher Si release. The LpSi8 remained stable, with no mineral transformations recorded even in the high Fe(II) treatment (Section S7). In these suspensions, mineral transformation was hindered by surface-adsorbed silicate in LpSi8, which reduced Fe(II) adsorption and hindered IAE (Figure 1).

The remaining ferrihydrite fractions at 4 weeks ranged between 56% (low Fe(II)) and 49% (high Fe(II)) for FhSi5 and between 100% (low Fe(II)) and 93% (high Fe(II)) for FhSi18, compared to 34% (low Fe(II)) and 35% (high Fe(II)) for pure Fh (Figure 2A,B,D,E and Section S7). The similar fractions of ferrihydrite remaining in comparable samples despite the increase in Fe(II)/Fe(III) ratios (from 0.2 to 2) indicate that the extent of ferrihydrite transformation was strongly influenced by the silicate loading of ferrihydrite, while the increase in the Fe(II) concentration had only a small effect.

In the FhSi18 suspension, ≥93% of the solid phase remained ferrihydrite even after 4 weeks of reaction in the low and the high Fe(II) treatment, yet Fe isotope data showed that FhSi18 underwent significant IAE (aqueous f^{57}Fe deviated <6% from f^{57}Fe of the total system after 4 weeks; Figure 1C,D). This indicates that mineral recrystallization of FhSi18 likely occurred despite the high silicate loading. Similar results were recorded for FhSi5, where within the first 2 h, the f^{57}Fe dropped sharply (to 6.9% in low Fe(II) and 36.6% in the high Fe(II) treatment), yet only ≤7% of FhSi5 transformed to lepidocrocite (Figures 1C,D and 2B,E and Section S7). During the recrystallization process, silicate seemed to hinder nucleation and crystal growth of goethite and magnetite, most likely by hindering the polymerization of iron octahedra.[24] This resulted in ferrihydrite and, at a low silicate content (FhSi5), lepidocrocite as the only mineral transformation products. Recent research suggests the formation of a labile Fe(III) species on the ferrihydrite surface.[9]

https://doi.org/10.1021/acs.est.1c08789
Environ. Sci. Technol. 2022, 56, 5929−5938

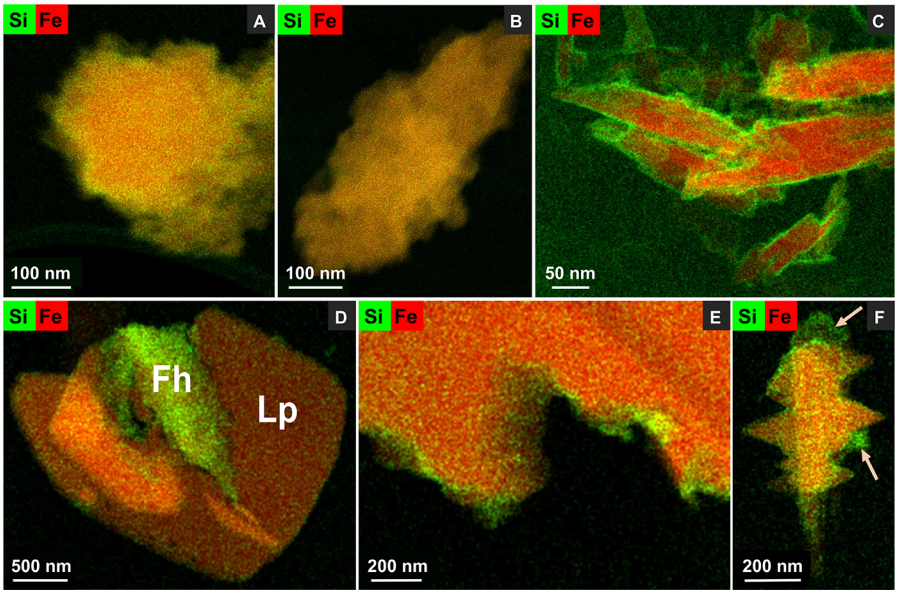

Figure 4. Elemental distribution maps of iron (Fe) and silicon (Si) in unreacted FhSi5 (A), FhSi18 (B) and LpSi8 (C), and in FhSi5 reacted with 0.3 mM Fe(II) (D, E) and reacted with 3 mM Fe(II) (F) for 4 weeks. Labels in panel (D) refer to the newly formed lepidocrocite (Lp) and remaining and/or recrystallized ferrihydrite (Fh). Arrows in panel (F) are pointing toward small platelets growing from a lath-like lepidocrocite. Corresponding HAADF images can be found in Section S9.

Considering this, silicate may have inhibited the polymerization of labile Fe(III) and therefore the formation of goethite and magnetite. Further, it has been shown that the presence of silicate can, depending on its concentration, hinder the precipitation of lepidocrocite and goethite, favoring ferrihydrite formation instead.[21,40] This is supported by Voegelin et al.[26] and Kaegi et al.[27] who demonstrated that abiotic Fe(II) oxidation at a Si/Fe ratio of 0.13 leads to the formation of poorly crystalline lepidocrocite (46%) mixed with a poorly crystalline silicate-rich hydrous ferric oxide phase (38%) and only small amounts of goethite (13%). They observed lepidocrocite formation only at initial aqueous Si/Fe ratios <0.24, suggesting that ferrihydrite and the silicate-rich hydrous ferric oxide phase precipitate until sufficient silicate has been removed from solution to enable lepidocrocite formation from excess Fe.[26] Thus, it is plausible that recrystallizing FhSi5 and FhSi18 continued to coprecipitate with aqueous silicate and continued to be stabilized against Fe(II)-catalyzed transformation, while lepidocrocite, if it forms, may only contain minor amounts of silicate.

Morphology of Transformation Products. The secondary electron images of 4-week reacted Fh (high Fe(II)) and FhSi5 (low and high Fe(II)) show that the morphology of lepidocrocite formed from Fe(II)-reacted ferrihydrite differed depending on the presence of both silicate and the spiked Fe(II) concentration (Figure 3A–F). With electron microscopy results, it needs to be considered that images can only represent a small fraction of the respective sample and therefore serve as indications. During the reaction of pure Fh in the high Fe(II) treatment, lepidocrocite crystallized as platelets and goethite formed clusters of small needles (Figure 3A), which agrees with previous observations for lepidocrocite[4,32] and goethite[4,14] morphology. In the presence of silicate, the reaction of FhSi5 in the low Fe(II) treatment led to large micrometer-sized lepidocrocite platelets (Figure 3C) and to large rectangular, thick platelets with rounded edges (Section S9). The latter contained spherical ferrihydrite particles inside and was covered by a smooth surface, which we suggest may be a crystallization front (Figure 3D and Section S9). The reaction of FhSi5 in the high Fe(II) treatment resulted in nanometer-sized lath-like lepidocrocites growing outward from ferrihydrite aggregates (Figure 3F) and independent, micrometer-sized, rough lath-like lepidocrocites with small, perpendicularly growing platelets (Figure 3E). These differences in morphology suggest that the growth of the lepidocrocite crystallites is strongly altered by the presence of silicate and Fe(II).[27]

The unreacted Lp consisted of finger-like structured small platelets with little morphological variation (Figure 3G). After the reaction in the high Fe(II) treatment, magnetite formed and residual lepidocrocite appeared shorter and thicker (Figure 3H). Southall et al.[41] and Joshi and Gorski[42] observed similar changes in goethite morphology during the reaction with Fe(II) and attributed this to preferential dissolution at goethite tips and preferential oxidation at long side edges. The secondary electron images of reacted and unreacted Lp suggest a similar mechanism for Lp during the interaction with Fe(II).

Morphological differences between the lepidocrocite crystallites formed via lepidocrocite synthesis versus through Fe(II)-catalyzed (Si-)ferrihydrite transformations were reflected in the crystallite thickness (Sections S8 and S9). Lepidocrocite thickness estimations were derived from fits of the 020 peak broadening in XRD patterns and refer to the crystal domain size perpendicular to the (010) plane[43] (details and the crystal structure in Section S6 and SEM images for comparison in Section S9). The thinnest lepidocrocite crystallites were observed for unreacted and Fe(II)-reacted Lp and LpSi8 (22–34 nm). In contrast, lepidocrocite crystallites that formed from FhSi5 in the low Fe(II) treatment were on average 185 nm thick, more than twice as thick as lepidocrocite crystallites formed from pure Fh (88 nm). This difference was less pronounced in the high Fe(II) treatment, where lepidocrocite crystallites at 4 weeks were only slightly thicker when formed from FhSi5 (87 nm) than when formed

https://doi.org/10.1021/acs.est.1c08789
Environ. Sci. Technol. 2022, 56, 5929–5938

from pure Fh (68 nm). The determination of the crystallite thickness of FhSi18-derived lepidocrocite was prevented by the small amount of lepidocrocite in the respective samples (<5%). The differences in thickness of lepidocrocite crystallites formed from Si-associated ferrihydrite (FhSi5) compared to pure Fh are likely related to the hindering effect of silicate on lepidocrocite crystallization.[21,26,27] The edge surfaces ((100) and (101)) of lepidocrocite platelets are the most proton-reactive and, therefore, are preferential adsorption sites for Fe(II)[44] and potentially also for silicate.[45] If adsorbed silicate blocks these reactive sites, then the lepidocrocite may be less reactive toward Fe(II) adsorption and oxidation. The face surfaces (010) of lepidocrocite platelets are less proton-reactive and are, in perfect crystals, not reactive at all since all surface groups are doubly coordinated ($\equiv Fe_2OH$).[44] However, mineral formation in the presence of impurities often leads to changes in the crystal structure,[46−49] and silicate has been reported to reduce linkages between FeO_6 octahedra in Fe oxyhydroxide polymeric complexes.[24] Therefore, for the lepidocrocite formed from FhSi5, the face surfaces (010) of the lepidocrocite platelets likely had more surface imperfections than lepidocrocite formed from pure Fh. This would suggest that the face surfaces (010) of the FhSi5-derived lepidocrocite platelets were more reactive toward Fe(II) adsorption and oxidation, promoting the lepidocrocite growth perpendicular to the face surface (010). This may explain the increase in the lepidocrocite thickness when formed from ferrihydrite silicate coprecipitates (FhSi5) during interactions with Fe(II). In summary, these findings suggest that coprecipitated silicate can lead to the formation of thicker lepidocrocite crystallites during Fe(II)-catalyzed transformation of ferrihydrite.

Silicate Redistribution within the Solid Phase. The elemental distribution maps of unreacted FhSi5 and FhSi18 showed that the distribution of Si and Fe was fairly homogeneous throughout the Fe mineral phases (Figure 4A,B and Section S9). This is in line with the Si-ferrihydrite coprecipitation process described by Dyer et al.[25] with silicate adsorbing to the rapidly forming small ferrihydrite particles prior to aggregation. In silicate-adsorbed lepidocrocite (LpSi8), Si was present on the lepidocrocite surfaces, with no separate Si-rich particles visible (Figure 4C).

After 4 weeks of reaction with 0.3 mM Fe(II), much more silicate was associated with ferrihydrite than with the newly formed lepidocrocite, resulting in an uneven Si distribution within the samples (compare Figure 4A with Figure 4D,E). The Si content was also lower in smooth surfaces on ferrihydrite aggregates compared to the rough, poorly crystalline edges and spherical ferrihydrite particles inside the aggregates (Figure 4E). In lepidocrocite formed from FhSi5 in the high Fe(II) treatment, Si was enriched in small platelets growing at the edge of the lath-like lepidocrocite, compared to the rest of the crystallite (Figure 4F). The Si distribution within residual FhSi5 or recrystallized ferrihydrite in the low Fe(II) treatment remained similarly even as in unreacted FhSi5 (Figure 4D). Generally, the lower content of Si in newly formed lepidocrocite than in initial FhSi5 agrees with the hindered crystallization of lepidocrocite at high Si/Fe ratios. This suggests that the retention of Si in the recrystallizing ferrihydrite enabled the formation of lepidocrocite from Fe(II)-reacted FhSi5.[26]

Environmental Implications. Our results demonstrate that coprecipitated silicate impacts the stability of ferrihydrite under reducing conditions without decreasing its reactivity in terms of Fe(II) adsorption, electron transfer, and atom exchange. Since aqueous silicate is, among other oxyanions, ubiquitous in soil and sediment pore waters (0.1−0.5 mM Si[50]), it can influence the formation and transformation of Fe oxyhydroxides in soils. This interaction leads to the formation of silicate-associated iron (oxy)hydroxides, e.g., ferrihydrite with common Si/Fe ratios of ∼0.1 and up to 0.35.[51,52] The outcomes of this study suggest that, especially at higher silicate loading (Si/Fe = 0.18), silicate can stabilize ferrihydrite against mineral transformation in soils under Fe-reducing conditions, allowing the persistence of ferrihydrite even under conditions where ferrihydrite would not be expected. At lower silicate contents (Si/Fe = 0.05), Si-ferrihydrite transformation can result in lepidocrocite, which not only can be stabilized by the small amounts of associated silicate but also forms imperfect crystallite surfaces, potentially providing more reactive surface sites. However, during Si-ferrihydrite transformation, Si redistribution can lead to the accumulation of silicate in recrystallizing ferrihydrite, further increasing the ferrihydrite stability. Additionally, this study shows that pure lepidocrocite may be more stable than previously assumed, if Fe(II) concentrations remain low. Alternatively, lepidocrocite may become inactivated by adsorbed silicate, which hindered Fe(II) adsorption and thus limited IAE. However, our results further suggest that ferrihydrite could act as a nucleation site for goethite in mixed mineral systems, potentially inducing lepidocrocite dissolution due to the greater thermodynamic stability of goethite. Collectively, these findings imply a dual role of silicate during the formation and transformation of Fe oxyhydroxides in soils, not only favoring ferrihydrite over lepidocrocite formation during the oxidation of Fe(II)[21,26,27] but also stabilizing both ferrihydrite and lepidocrocite against mineral transformation under Fe-reducing conditions. Because Fe oxyhydroxides are important sorbent phases that influence the biogeochemical cycling of nutrients and contaminants, the altered mineral transformation dynamics in the presence of silicate anions need to be considered when assessing the iron mineralogy in Fe-reducing soil environments.

■ ASSOCIATED CONTENT

Supporting Information

The Supporting Information is available free of charge at https://pubs.acs.org/doi/10.1021/acs.est.1c08789.

Further details for material and methods and additional data and figures supporting the results and discussion (PDF)

■ AUTHOR INFORMATION

Corresponding Author

Laurel K. ThomasArrigo − *Soil Chemistry Group, Institute of Biogeochemistry and Pollutant Dynamics, Department of Environmental Systems Science, ETH Zürich, 8092 Zürich, Switzerland;* orcid.org/0000-0002-6758-3760; Email: laurel.thomas@usys.ethz.ch

Authors

Katrin Schulz − *Soil Chemistry Group, Institute of Biogeochemistry and Pollutant Dynamics, Department of Environmental Systems Science, ETH Zürich, 8092 Zürich, Switzerland;* orcid.org/0000-0001-9608-0882

https://doi.org/10.1021/acs.est.1c08789
Environ. Sci. Technol. 2022, 56, 5929−5938

Ralf Kaegi − *Eawag, Swiss Federal Institute of Aquatic Science and Technology, 8060 Dübendorf, Switzerland;* orcid.org/0000-0002-2430-4733

Ruben Kretzschmar − *Soil Chemistry Group, Institute of Biogeochemistry and Pollutant Dynamics, Department of Environmental Systems Science, ETH Zürich, 8092 Zürich, Switzerland;* orcid.org/0000-0003-2587-2430

Complete contact information is available at: https://pubs.acs.org/10.1021/acs.est.1c08789

Notes

The authors declare no competing financial interest.

■ ACKNOWLEDGMENTS

We are grateful to Kurt Barmettler, Sylvain Bouchet, Joëlle Kubeneck, Sandra Heller, Michael Plötze, Annette Röthlisberger, and Marion Rothaupt (ETH Zürich) for assisting with laboratory analyses. We acknowledge the Scientific Center for Optical and Electron Microscopy (ScopeM) of the ETH Zürich for providing access to their microscopes. Further, we thank the three anonymous reviewers and the associate editor for their helpful comments, which greatly improved this manuscript. This work received funding from the European Research Council (ERC) under the European Union's Horizon 2020 research and innovation programme (grant agreement no. 788009-IRMIDYN-ERC-2017-ADG).

■ REFERENCES

(1) Cornell, R. M.; Schwertmann, U. *The Iron Oxides*; Wiley: Weinheim, Germany, 2003.

(2) Couture, R.-M.; Charlet, L.; Markelova, E.; Madé, B.; Parsons, C. T. On-off Mobilization of Contaminants in Soils during Redox Oscillations. *Environ. Sci. Technol.* **2015**, *49*, 3015−3023.

(3) Weber, F. A.; Voegelin, A.; Kretzschmar, R. Multi-Metal Contaminant Dynamics in Temporarily Flooded Soil under Sulfate Limitation. *Geochim. Cosmochim. Acta* **2009**, *73*, 5513−5527.

(4) Hansel, C. M.; Benner, S. G.; Fendorf, S. Competing Fe(II)-Induced Mineralization Pathways of Ferrihydrite. *Environ. Sci. Technol.* **2005**, *39*, 7147−7153.

(5) Boland, D. D.; Collins, R. N.; Miller, C. J.; Glover, C. J.; Waite, T. D. Effect of Solution and Solid-Phase Conditions on the Fe(II)-Accelerated Transformation of Ferrihydrite to Lepidocrocite and Goethite. *Environ. Sci. Technol.* **2014**, *48*, 5477−5485.

(6) Pedersen, H. D.; Postma, D.; Jakobsen, R.; Larsen, O. Fast Transformation of Iron Oxyhydroxides by the Catalytic Action of Aqueous Fe(II). *Geochim. Cosmochim. Acta* **2005**, *69*, 3967−3977.

(7) Williams, A. G. B.; Scherer, M. M. Spectroscopic Evidence for Fe(II)-Fe(III) Electron Transfer at the Iron Oxide-Water Interface. *Environ. Sci. Technol.* **2004**, *38*, 4782−4790.

(8) Handler, R. M.; Beard, B. L.; Johnson, C. M.; Scherer, M. M. Atom Exchange between Aqueous Fe(II) and Goethite: An Fe Isotope Tracer Study. *Environ. Sci. Technol.* **2009**, *43*, 1102−1107.

(9) Sheng, A.; Liu, J.; Li, X.; Qafoku, O.; Collins, R. N.; Jones, A. M.; Pearce, C. I.; Wang, C.; Ni, J.; Lu, A.; Rosso, K. M. Labile Fe(III) from Sorbed Fe(II) Oxidation Is the Key Intermediate in Fe(II)-Catalyzed Ferrihydrite Transformation. *Geochim. Cosmochim. Acta* **2020**, *272*, 105−120.

(10) Aeppli, M.; Kaegi, R.; Kretzschmar, R.; Voegelin, A.; Hofstetter, T. B.; Sander, M. Electrochemical Analysis of Changes in Iron Oxide Reducibility during Abiotic Ferrihydrite Transformation into Goethite and Magnetite. *Environ. Sci. Technol.* **2019**, *53*, 3568−3578.

(11) Liu, H.; Li, P.; Zhu, M.; Wei, Y.; Sun, Y. Fe(II)-Induced Transformation from Ferrihydrite to Lepidocrocite and Goethite. *J. Solid State Chem.* **2007**, *180*, 2121−2128.

(12) Sheng, A.; Liu, J.; Li, X.; Luo, L.; Ding, Y.; Chen, C.; Zhang, X.; Wang, C.; Rosso, K. M. Labile Fe(III) Supersaturation Controls Nucleation and Properties of Product Phases from Fe(II)-Catalyzed Ferrihydrite Transformation. *Geochim. Cosmochim. Acta* **2021**, *309*, 272−285.

(13) ThomasArrigo, L. K.; Byrne, J. M.; Kappler, A.; Kretzschmar, R. Impact of Organic Matter on Iron(II)-Catalyzed Mineral Transformations in Ferrihydrite−Organic Matter Coprecipitates. *Environ. Sci. Technol.* **2018**, *52*, 12316−12326.

(14) Yan, W.; Liu, H.; Chen, R.; Xie, J.; Wei, Y. Dissolution and Oriented Aggregation: Transformation from Lepidocrocite to Goethite by the Catalysis of Aqueous Fe(II). *RSC Adv.* **2015**, *5*, 106396−106399.

(15) Tamaura, Y.; Ito, K.; Katsura, T. Transformation of γ-FeO(OH) to Fe_3O_4 by Adsorption of Iron(II) on γ-FeO(OH). *J. Chem. Soc., Dalton Trans.* **1983**, 189−194.

(16) Masue-Slowey, Y.; Loeppert, R. H.; Fendorf, S. Alteration of Ferrihydrite Reductive Dissolution and Transformation by Adsorbed As and Structural Al: Implications for As Retention. *Geochim. Cosmochim. Acta* **2011**, *75*, 870−886.

(17) Borch, T.; Masue, Y.; Kukkadapu, R.; Fendorf, S. Phosphate Imposed Limitations on Biological Reduction and Alteration of Ferrihydrite. *Environ. Sci. Technol.* **2007**, *41*, 166−172.

(18) Jones, A. M.; Collins, R. N.; Rose, J.; Waite, T. D. The Effect of Silica and Natural Organic Matter on the Fe(II)-Catalysed Transformation and Reactivity of Fe(III) Minerals. *Geochim. Cosmochim. Acta* **2009**, *73*, 4409−4422.

(19) Cismasu, A. C.; Michel, F. M.; Tcaciuc, A. P.; Brown, G. E. Properties of Impurity-Bearing Ferrihydrite III. Effects of Si on the Structure of 2-Line Ferrihydrite. *Geochim. Cosmochim. Acta* **2014**, *133*, 168−185.

(20) Chen, C.; Kukkadapu, R.; Sparks, D. L. Influence of Coprecipitated Organic Matter on Fe^{2+}(Aq)-Catalyzed Transformation of Ferrihydrite: Implications for Carbon Dynamics. *Environ. Sci. Technol.* **2015**, *49*, 10927−10936.

(21) Schwertmann, U.; Thalmann, H. The Influence of [Fe(II)], [Si], and pH on the Formation of Lepidocrocite and Ferrihydrite during Oxidation of Aqueous $FeCl_2$ Solutions. *Clay Miner.* **1976**, *11*, 189−200.

(22) Hiemstra, T. Ferrihydrite Interaction with Silicate and Competing Oxyanions: Geometry and Hydrogen Bonding of Surface Species. *Geochim. Cosmochim. Acta* **2018**, *238*, 453−476.

(23) Dyer, L. G.; Fawell, P. D.; Newman, O. M. G.; Richmond, W. R. Synthesis and Characterisation of Ferrihydrite/Silica Co-Precipitates. *J. Colloid Interface Sci.* **2010**, *348*, 65−70.

(24) Pokrovski, G. S.; Schott, J.; Farges, F.; Hazemann, J. L. Iron (III)-Silica Interactions in Aqueous Solution: Insights from X-Ray Absorption Fine Structure Spectroscopy. *Geochim. Cosmochim. Acta* **2003**, *67*, 3559−3573.

(25) Dyer, L. G.; Chapman, K. W.; English, P.; Saunders, M.; Richmond, W. R. Insights into the Crystal and Aggregate Structure of Fe^{3+} Oxide/Silica Co-Precipitates. *Am. Mineral.* **2012**, *97*, 63−69.

(26) Voegelin, A.; Kaegi, R.; Frommer, J.; Vantelon, D.; Hug, S. J. Effect of Phosphate, Silicate, and Ca on Fe(III)-Precipitates Formed in Aerated Fe(II)- and As(III)-Containing Water Studied by X-ray Absorption Spectroscopy. *Geochim. Cosmochim. Acta* **2010**, *74*, 164−186.

(27) Kaegi, R.; Voegelin, A.; Folini, D.; Hug, S. J. Effect of Phosphate, Silicate, and Ca on the Morphology, Structure and Elemental Composition of Fe(III)-Precipitates Formed in Aerated Fe(II) and As(III) Containing Water. *Geochim. Cosmochim. Acta* **2010**, *74*, 5798−5816.

(28) Taylor, P. D. P.; Maeck, R.; De Bièvre, P. Determination of the Absolute Isotopic Composition and Atomic Weight of a Reference Sample of Natural Iron. *Int. J. Mass Spectrom. Ion Processes* **1992**, *121*, 111−125.

(29) Schwertmann, U.; Cornell, R. M. *Iron Oxides in the Laboratory: Synthesis and Preparation*; John Wiley & Sons, 1991.

(30) Hofmann, A.; Pelletier, M.; Michot, L.; Stradner, A.; Schurtenberger, P.; Kretzschmar, R. Characterization of the Pores in

Hydrous Ferric Oxide Aggregates Formed by Freezing and Thawing. *J. Colloid Interface Sci.* **2004**, *271*, 163−173.
(31) Brunauer, S.; Emmett, P. H.; Teller, E. Adsorption of Gases in Multimolecular Layers. *J. Am. Chem. Soc.* **1938**, *60*, 309−319.
(32) ThomasArrigo, L. K.; Kaegi, R.; Kretzschmar, R. Ferrihydrite Growth and Transformation in the Presence of Ferrous Iron and Model Organic Ligands. *Environ. Sci. Technol.* **2019**, *53*, 13636−13647.
(33) Walter, W. G. Standard Methods for the Examination of Water and Wastewater (11th Ed.). *Am. J. Public Heal. Nations Heal* **1961**, *51*, 940−940.
(34) Scarlett, N. V. Y.; Madsen, I. C. Quantification of Phases with Partial or No Known Crystal Structures. *Powder Diffr.* **2006**, *21*, 278−284.
(35) Hansel, C. M.; Benner, S. G.; Neiss, J.; Dohnalkova, A.; Kukkadapu, R.; Fendorf, S. Secondary Mineralization Pathways Induced by Dissimilatory Iron Reduction of Ferrihydrite under Advective Flow. *Geochim. Cosmochim. Acta* **2003**, *67*, 2977−2992.
(36) Frierdich, A. J.; Saxey, D. W.; Adineh, V. R.; Fougerouse, D.; Reddy, S. M.; Rickard, W. D. A.; Sadek, A. Z.; Southall, S. C. Direct Observation of Nanoparticulate Goethite Recrystallization by Atom Probe Analysis of Isotopic Tracers. *Environ. Sci. Technol.* **2019**, *53*, 13126−13135.
(37) Handler, R. M.; Frierdich, A. J.; Johnson, C. M.; Rosso, K. M.; Beard, B. L.; Wang, C.; Latta, D. E.; Neumann, A.; Pasakarnis, T. S.; Premaratne, W. A. P. J.; Scherer, M. M. Fe(II)-Catalyzed Recrystallization of Goethite Revisited. *Environ. Sci. Technol.* **2014**, *48*, 11302−11311.
(38) Frierdich, A. J.; Helgeson, M.; Liu, C.; Wang, C.; Rosso, K. M.; Scherer, M. M. Iron Atom Exchange between Hematite and Aqueous Fe(II). *Environ. Sci. Technol.* **2015**, *49*, 8479−8486.
(39) Liu, J.; Sheng, A.; Li, X.; Arai, Y.; Ding, Y.; Nie, M.; Yan, M.; Rosso, K. M. Understanding the Importance of Labile Fe(III) during Fe(II)-Catalyzed Transformation of Metastable Iron Oxyhydroxides. *Environ. Sci. Technol.* **2022**, *56*, 3801.
(40) Wang, X.; Zhu, M.; Lan, S.; Ginder-Vogel, M.; Liu, F.; Feng, X. Formation and Secondary Mineralization of Ferrihydrite in the Presence of Silicate and Mn(II). *Chem. Geol.* **2015**, *415*, 37−46.
(41) Southall, S. C.; Micklethwaite, S.; Wilson, S. A.; Frierdich, A. J. Changes in Crystallinity and Tracer-Isotope Distribution of Goethite during Fe(II)-Accelerated Recrystallization. *ACS Earth Space Chem.* **2018**, *2*, 1271−1282.
(42) Joshi, P.; Gorski, C. A. Anisotropic Morphological Changes in Goethite during Fe^{2+}-Catalyzed Recrystallization. *Environ. Sci. Technol.* **2016**, *50*, 7315−7324.
(43) Schulze, D. G.; Schwertmann, U. The Influence of Aluminium on Iron Oxides: X. Properties of Al-Substituted Goethites. *Clay Miner.* **1984**, *19*, 521−539.
(44) Hiemstra, T.; van Riemsdijk, W. H. Adsorption and Surface Oxidation of Fe(II) on Metal (Hydr)Oxides. *Geochim. Cosmochim. Acta* **2007**, *71*, 5913−5933.
(45) Kanematsu, M.; Waychunas, G. A.; Boily, J. F. Silicate Binding and Precipitation on Iron Oxyhydroxides. *Environ. Sci. Technol.* **2018**, *52*, 1827−1833.
(46) Eusterhues, K.; Wagner, F. E.; Häusler, W.; Hanzlik, M.; Knicker, H.; Totsche, K. U.; Kögel-Knabner, I.; Schwertmann, U. Characterization of Ferrihydrite-Soil Organic Matter Coprecipitates by X-ray Diffraction and Mössbauer Spectroscopy. *Environ. Sci. Technol.* **2008**, *42*, 7891−7897.
(47) Murad, E.; Schwertmann, U. The Influence of Aluminium Substitution and Crystallinity on the Mössbauer Spectra of Goethite. *Clay Miner.* **1983**, *18*, 301−312.
(48) Liao, S.; Wang, X.; Yin, H.; Post, J. E.; Yan, Y.; Tan, W.; Huang, Q.; Liu, F.; Feng, X. Effects of Al Substitution on Local Structure and Morphology of Lepidocrocite and Its Phosphate Adsorption Kinetics. *Geochim. Cosmochim. Acta* **2020**, *276*, 109−121.
(49) Schwertmann, U.; Wolska, E. The Influence of Aluminum on Iron Oxides. XV. Al-for-Fe Substitution in Synthetic Lepidocrocite. *Clays Clay Miner.* **1990**, *38*, 209−212.
(50) Sommer, M.; Kaczorek, D.; Kuzyakov, Y.; Breuer, J. Silicon Pools and Fluxes in Soils and Landscapes - A Review. *J. Plant Nutr. Soil Sci.* **2006**, *169*, 310−329.
(51) Parfitt, R. L.; Van Der Gaast, S. J.; Childs, C. W. A Structural Model for Natural Siliceous Ferrihydrite. *Clays Clay Miner.* **1992**, *40*, 675−681.
(52) Childs, C. W. Ferrihydrite: A Review of Structure, Properties and Occurrence in Relation to Soils. *J. Plant Nutr. Soil Sci.* **1992**, *155*, 441−448.

https://doi.org/10.1021/acs.est.1c08789
Environ. Sci. Technol. 2022, 56, 5929−5938